Molecular Dynamics Simulations of PEI Mediated DNA Aggregation

Chongbo Sun,[†] Tian Tang,*[,†] and Hasan Uludağ[‡,§,⊥]

[†]Department of Mechanical Engineering, University of Alberta, Edmonton, AB, Canada T6G 2G8

[‡]Department of Chemical and Materials Engineering, University of Alberta, Edmonton, AB, Canada T6G 2G6

[§]Department of Biomedical Engineering, University of Alberta, Edmonton, AB, Canada T6G 2V2

[⊥]Faculty of Pharmacy and Pharmaceutical Sciences, University of Alberta, Edmonton, AB, Canada T6G 2N8

Ⓢ *Supporting Information*

ABSTRACT: Understanding the molecular mechanism of polycation induced DNA aggregation and condensation is important for optimal design of gene delivery carriers. In this work, we performed a series of all-atom molecular dynamics (MD) simulations to investigate polyethylenimine (PEI) mediated DNA aggregation. We found that PEIs condense DNA through two mechanisms: polyion bridging and electrostatic screening of the DNA charges. At PEI/DNA charge ratio >1, PEIs can completely neutralize DNAs at a short distance (~12 Å from the C1′ atoms), and this distance is found to be insensitive to the exact value of the charge ratio.

When excess PEIs are added to a formed DNA−PEI aggregate, they are found to bind to the aggregate and increase its cationic charge. The added PEIs can also replace the PEIs previously bound to the aggregate. The excess PEIs, however, do not change the spacing of the DNAs in the aggregates. Our simulation results shed light on the mechanisms of PEI, and more generally polycation, mediated DNA aggregation and condensation.
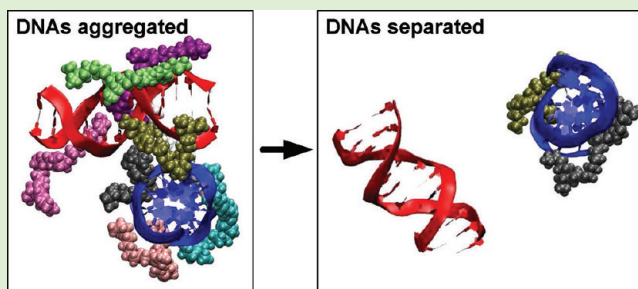
1. INTRODUCTION

DNA condensation has been studied for many years due to its fundamental biological importance, such as the tight packaging of DNA in the chromatin structure and its regulation.[1] More recently, great interest in nonviral gene delivery for therapeutic purposes has stimulated development of systems that can condense DNA and package it suitable for cellular uptake.[2] It was experimentally found that multivalent ions can induce DNA condensation while monovalent or divalent ions lack this capability. Certain synthetic cationic polymers such as poly-ethylenimine (PEI) can condense nucleic acids into nano-particulate aggregates and have been employed as effective gene carriers.[3,4] The compactness and stability of the formed nanoparticulate aggregates were found to be relevant to the delivery efficacy; more stable polymer formulations were correlated with better uptake into cells and, ultimately, better gene expression.[5,6] The ratio of polymer (e.g., PEI) to DNA in the aggregate formation is known to be critical for trans-fection;[7,8] excess PEI gives the aggregates an overall positive charge for increased interaction with membranes and contributes favorably to cell modifications. Several experimental tools are available for the study of aggregate physical features and overall stability.[9] However, little is known about the structures of DNA/polymer complexes at the atomistic level due to limitations of the experimental tools. The role of polymeric cations in maintaining the aggregates stability as well as molecular kinetics in such aggregates remains to be probed.

DNA is a highly charged polyelectrolyte with a charge density of $-2e/3.4$ Å. Mean-field theory such as Poisson–Boltzmann equation always predicts a repulsive interaction between like-charged polyelectrolytes and thus cannot explain the multivalent ion induced DNA condensation. Coarse grained simulations of polyelectrolytes normally treat several or tens of atoms on the polyelectrolytes as a unit and water as a continuous dielectric medium. This method has been employed in the past decade to study oppositely charged polyelectrolyte interactions[10−16] and had some success in predicting how chain length, charge density, charge ratio, and ion concentration affect the complexation of polycation and polyanion. However, coarse grained simulations neglect the fine details of the molecules, especially the water structure around the binding sites, and thus are only appropriate for interactions over distances exceeding the atomic scale. In the case of polymer mediated DNA aggregation, the surfaces of the DNA segments can be as close as a few angstroms.[17] In such situations, water molecules play a crucial role in arranging their structure (polarity) to mediate the strong electrostatic interaction and to form hydrogen bonds; thus, an atomistic description is necessary in order to understand polycation induced DNA aggregation. Recent experiments have also demonstrated the crucial role of atomic topologies in strong polyelectrolyte

interactions. For example, it was found that double-stranded RNA resists condensation by trivalent counterions, which can otherwise condense double-stranded DNA,[18] and divalent counterions can condense triple-stranded DNA but lack the capability to condense double-stranded DNA.[19] These findings further underline the requirement to incorporate an all-atom representation in simulating polycation mediated nucleic acids aggregation and condensation. Atomic simulations have recently been employed to study the complexation of single nucleic acid molecule with polycations,[20−27] where the structure, dynamics, and energetics of the nucleic acid/polycation complexes were investigated, but studies investigating polycation mediated aggregation of multiple DNAs are yet missing.

In this work, we performed a series of large scale all-atom molecular dynamics (MD) simulations to study the PEI mediated DNA aggregation. Specifically, we studied the mechanism and dynamics of PEI induced DNA aggregation, how close the DNA segments are in the DNA/PEI polyplex, and how the compactness of the DNAs is affected by the DNA/PEI charge ratio. The PEI studied in this work is a 568 Da low molecular weight (LMW) PEI. Such LMW PEIs provide an optimal system size that can be simulated by all-atom MD and are increasingly employed as gene delivery carriers due to suitable compatibility with cellular systems.[7,28,29] To our knowledge, this study is the first atomistic simulations on polycation mediated DNA aggregation involving multiple DNA molecules. The results help to elucidate on the mechanism of PEI mediated DNA aggregation at the atomic resolution and, moreover, to understand DNA aggregation and condensation involving other polycations of similar characteristics.

2. METHODS

The DNA simulated in this work was a Drew−Dickerson dodecamer d(CGCGAATTCGCG)$_2$ composed of 24 nucleotides, which carries a total charge of −22 in the fully deprotonated state. The PEI simulated was a branched PEI consisting of 13 amine groups with a molecular weight of 568 Da. The chemical structure and protonation sites of the PEI are shown in Figure 1. We chose to have 6 amine groups
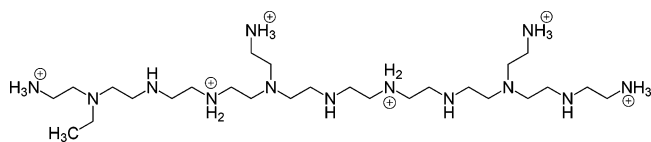
Figure 1. Molecular structure and protonation sites of the PEI studied.

protonated (46% protonated) to be consistent with the protonation ratio of 47% for 600 Da PEI from our recent study.[30] The protonation sites were assigned to both the primary and secondary amines and were distributed as uniformly as possible to minimize thermodynamic interactions between the protonated amines.[31] An MD simulation was first performed for 6 ns for PEI surrounded by explicit water and counterions, and the configuration of the PEI at the end of the simulation was adopted as the initial configurations for PEIs in the complex formation simulations.[31] Seven separate systems were simulated in this study, and their information is summarized in Table 1. Each system consists of a certain number of DNA(s), PEIs, ions, and water molecules. Details of the simulated systems and the explanations on their designations are given below.

2.1. Simulated Systems and Procedure. The first two systems shown in Table 1, namely D-4P and D-8P, each contains a single DNA and multiple PEIs, 4 PEIs in D-4P, and 8 PEIs in D-8P. For each

system, the principal axes of the PEIs were initially aligned parallel to the DNA axis, and the center of mass (COM) of each PEI was positioned at 25 Å away from the DNA COM. Each system was simulated for 100 ns, and in both cases, four PEIs were attached to the DNA at the late stage of the simulations.[32] The structure of the D-4P system at 15 ns was then used to construct the systems that involve multiple DNAs to study the DNA aggregation. The D-4P and D-8P systems are also discussed in section 3.2 to address the ability of PEI to neutralize DNA.

To study the PEI-mediated aggregation of multiple DNA molecules, we first simulated two systems, named 2D-8P-50 and 2D-8P (Table 1), each containing two DNAs and eight PEIs. The initial configurations of these two systems were constructed by solvating two identical D-4P complexes in the simulation box, as shown in Figures 2a and 2b, respectively. The axes of the DNAs in the two complexes were aligned to be parallel, and the COM of the two complexes were initially separated by 50 Å in 2D-8P-50 and by 32 Å in 2D-8P. The distinction between these two systems is marked by the "50" in the name of system 2D-8P-50, which refers to the initial separation of 50 Å between the two D-4P complexes. The reason for using two different COM distances was to examine the likelihood of aggregation at these separations.

Another simulation was conducted for a system that consists of two DNAs and two PEIs, indicated by 2D-2P in Table 1. While the 2D-8P-50 and 2D-8P systems both have a PEI/DNA charge ratio of ∼1/1, the 2D-2P system has a PEI/DNA charge ratio that is much smaller than one (∼1/4). Hence, simulation on this system allows us to investigate the effect of electrostatic screening by PEI on DNA aggregation. The initial configuration of 2D-2P is based on the configuration of 2D-8P at 100 ns of its simulation. Specifically, as will be discussed later, we found that two out of the eight PEIs in 2D-8P are bridging the two DNAs at the end of the simulation. We kept these two PEIs and removed the other six PEIs. 36 Na$^+$ ions were assigned on the locations of the protonated nitrogens on the removed 6 PEIs. The initial configuration of the 2D-2P system is illustrated in Figure 2c.

To further study the formation of aggregate in the case of multiple DNA segments, we performed a simulation on a system with 4 DNAs and 16 PEIs, named 4D-16P in Table 1. In constructing the initial configuration for 4D-16P, we followed a similar procedure to that of 2D-8P. In particular, we adopted four D-4P complexes and arranged them on the four corners of a square, as shown in Figure 2d. The axes of the four DNAs were aligned to be parallel, and the COM of each D-4P complex was separated from the COM of its neighboring complex by 35 Å.

To investigate the effect of excess PEIs on the DNA aggregation, 12 PEIs were added to the 4D-16P system at the simulation time of 100 ns, and the new system is referred to as 4D-28P. The added 12 PEIs surrounded the 4D-16P complex in a circular fashion, with 8 PEIs located at 42 Å from the COM of 4D-16P and 4 PEIs located at 50 Å from the COM of 4D-16P. The initial configuration of 4D-28P is shown in Figure 2e.

2.2. Simulation Details. A CHARMM format force field was devised for PEI based on the CHARMM General Force Field,[33] and CHARMM 27 force field[34,35] was used for all other molecules. The force field parameters for PEI have been carefully validated through *ab initio* calculations, a study on sensitivity of MD results to torsional parameters, and comparison with previous works.[31] The simulations were performed using MD package NAMD.[36] TIP3P water model,[37] periodic boundary condition, and full electrostatics with particle-mesh Ewald method[38] were used for all the simulations. A cutoff of 12 Å was used for van der Waals interactions and electrostatics pairwise calculations. All bonds containing hydrogen atoms were constrained using the SHAKE algorithm[39] during all the simulations, and a time step of 2 fs was used.

For each system described in section 2.1, the DNA(s) and PEIs were solvated into a water box, the size of which was set to be large enough to make sure the DNA(s) and PEIs are at least 36 Å away from their nearest periodic images in each direction. Ions (numbers summarized in Table 1) were then added to the water box by randomly replacing the same number of water molecules using

Table 1. Information on the Seven Different Systems Simulated in This Study

system name	no. of DNA/PEI	charge ratio DNA/PEI	no. of atoms	size of simulation box (Å^3)	no. of Na$^+$/Cl$^-$	simulation time (ns)
D-4P	1/4	22/24	43 244	74 × 79 × 74	0/2	100
D-8P	1/8	22/48	60 882	88 × 93 × 73	0/26	100
2D-8P-50	2/8	44/48	77 149	122 × 78 × 79	0/4	100
2D-8P	2/8	44/48	65 965	105 × 78 × 79	0/4	100
2D-2P	2/2	44/12	64 423	104 × 78 × 79	36/4	200
4D-16P	4/16	88/96	97 007	107 × 112 × 79	0/8	130
4D-28P	4/28	88/168	175 910	117 × 122 × 120	0/80	200
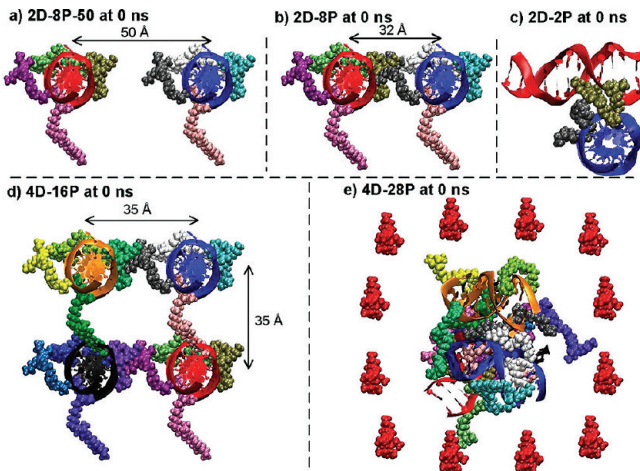
Figure 2. Initial configurations of the systems: (a) 2D-8P-50, (b) 2D-8P, (c) 2D-2P, (d) 4D-16P, (e) 4D-28P. Different PEIs are represented in different colors (except in (e) where the extra 12 PEIs are in red); water and ions are removed for clarity.

VMD.[40] During each simulation, the system was first minimized for 2000 steps with DNA(s)/PEIs fixed, and then 2000 steps with DNA(s)/PEIs non-hydrogen atoms harmonically restrained, followed by 1000 steps of unrestrained minimization. The system was then gradually heated from 0 to 300 K in 20 ps with 10 kcal/mol × Å^2 harmonic restraint on the DNA(s)/PEIs non-hydrogen atoms. The restraint was kept on for another 4 ns at 300 K and 1 bar to relax the ions around the solutes. The restraint was then removed, and NPT ensemble simulation was performed for 100−200 ns (simulation time for each system shown in Table 1). VMD[40] was used for visualization and trajectories analysis.

2.3. Definitions and Acronyms. To facilitate the discussion of the simulation results, we introduced the following definitions and acronyms in analyzing the simulation trajectories.

In systems 2D-8P and 4D-16P, each DNA is labeled with a capital letter (A, B, C, or D), and the four PEIs initially associated with the DNA in a D-4P complex (see section 2.1) are labeled with the same capital letter plus a number. For example, "A1, A2, A3, A4" stand for the four PEIs initially associated with DNA molecule A. In system 4D-28P, we keep the same labels for the 16 PEIs from 4D-16P and label the extra 12 PEIs by "E1−E12". The acronyms for the DNAs and PEIs in each system are summarized in Table 2.

Table 2. Acronyms of the DNAs and PEIs in Each System

system	DNAs	PEIs
2D-8P	A, B	A1−A4, B1−B4
2D-2P	A, B	A1, B4
4D-16P	A, B, C, D	A1−A4, B1−B4, C1−C4, D1−D4
4D-28P	A, B, C, D	A1−A4, B1−B4, C1−C4, D1−D4, E1−E12

To describe the binding state of PEI to DNA, a PEI N is said to be "in close contact with the DNA" if it is within 4 Å of any N/O atoms
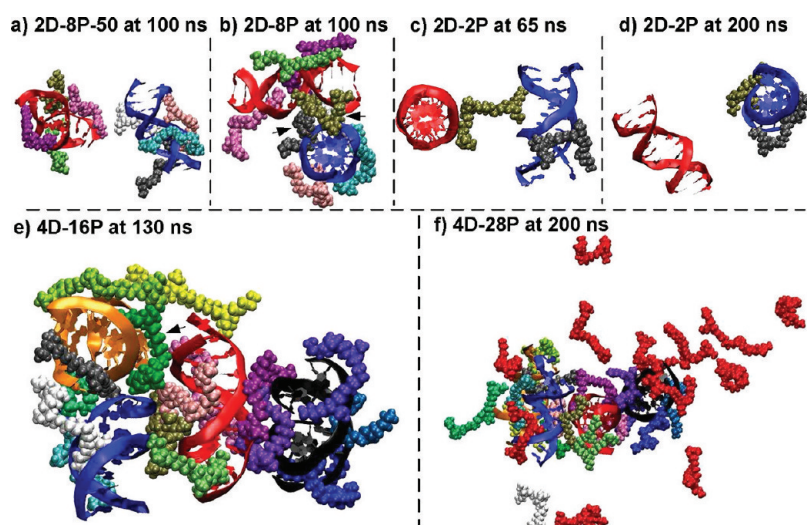
of the DNA. We chose 4 Å because this is the distance within which the PEI amine groups can form direct hydrogen bond with the DNA.[31] A PEI is said to be "bound" to a DNA molecule if it has at least one N in close contact with this DNA. If a PEI is "bound" to two or more DNA molecules simultaneously, this PEI is said to be bridging or forming a polyion bridge between the DNAs.

To investigate the DNA−DNA spacing in the aggregates, we defined the "shortest distance" and "root-mean-square (rms) distance" between two DNA molecules. We first represent each DNA as a series of points each being the COM of a Watson−Crick DNA base pair (see Figure S2 in Supporting Information). For each dodecamer studied in this work, there are 12 such points, and connecting neighboring points results in 11 segments. For a pair of segments from two different DNAs, we can calculate their shortest distance, and there are 121 such distances (d_i, i = 1...121) between all pairs of segments from the two DNA dodecamers. We defined the minimum of these 121 distances as the "shortest distance" $d_{shortest}$ and the root-mean-square of these 121 distances as the "rms distance" d_{rms} ($d_{rms} = [(\sum_{i=1}^{121} d_i^2)/121]^{1/2}$). "Shortest distance" is a parameter to quantify the closet approach of two DNA molecules, whereas "rms distance" is a parameter to characterize the closeness of two DNA molecules as two entities.

3. RESULTS AND DISCUSSION

For the system 2D-8P-50, the two D-4P complexes stayed separate during the 100 ns simulation. Figure 3a shows the configuration of 2D-8P-50 at the end of the simulation, where the two DNAs are separated at a COM distance of ∼42 Å. No PEI molecule simultaneously binds to both DNAs. We attribute the lack of aggregation in this case to the fact that the two D-4P complexes were initially separated by a relatively large distance; namely, each complex is 50 Å from its closest complex and 72 Å from its second closest complex as a periodic image. Because each D-4P complex carries a total charge of +2, an overall repulsive electrostatic interaction between the two complexes is expected. A sufficiently close approach might be necessary to allow the attractive interaction between the positively and negatively charged parts of the complexes to form an aggregate. Although sufficient diffusion of the macromolecular complexes could accomplish this, the 100 ns simulation time was relatively short, so that the diffusion alone apparently did not bring the two complexes close enough to form an aggregate in the 2D-8P-50 system. To obtain an aggregate within a practical simulation time, we brought the D-4P complexes at shorter separations of 32 Å for the 2D-8P system and 35 Å for the 4D-16P system at the beginning of the simulations. In both cases, aggregation happened shortly after the simulation started, and the complexes were never separated again thereafter (see movies "2D-8P.mpg" and "4D-16P.mpg" in Supporting Information). The overall repulsive electrostatic interaction was therefore not an impediment for aggregate formation. In the following subsections, structural analysis were conducted to examine the mechanism of aggregation and to characterize the formed aggregates.

a) 2D-8P-50 at 100 ns b) 2D-8P at 100 ns c) 2D-2P at 65 ns   d) 2D-2P at 200 ns

**e) 4D-16P at 130 ns**   **f) 4D-28P at 200 ns**

Figure 3. Snapshots of the systems in the simulations: (a) 2D-8P-50 at 100 ns, (b) 2D-8P at 100 ns, (c) 2D-2P at 65 ns, (d) 2D-2P at 200 ns, (e) 4D-16P at 130 ns, and (f) 4D-28P at 200 ns. Different PEIs are represented in different colors (except in (f) where the added 12 PEIs are in red); water and ions are removed for clarity.

3.1. Mechanism of Aggregation. Figure 3b shows the conformation of the system 2D-8P at the last stage of the 100 ns simulation. It can be seen that all eight PEIs are attached to the DNAs with significant fraction of each PEI in contact with the DNAs. Two PEIs (indicated by the two black arrows in Figure 3b) bind to the two DNAs concurrently, bridging them so that they are closer to each other compared with the initial configuration. Figure 3e is the snapshot of the 4D-16P system at the end of its simulation. As in the 2D-8P system, all PEIs are attached to the DNAs, and about half of the PEIs participate in bridging the DNA molecules. In particular, one PEI (indicated by the black arrow in Figure 3e) binds to three DNAs simultaneously.

To quantify the ability of PEI to bridge the DNA molecules, we plotted the binding state of individual PEIs to each DNA in terms of the number of Ns from each PEI in close contact with each DNA (see section 2.3 for definition of "close contact"), as shown in Figure 4 for the 2D-8P system and in Figure 5 for the 4D-16P system. In Figure 4, each subfigure corresponds to one of the 8 PEIs in the 2D-8P system and contains two curves, each of which describes the number of Ns of this PEI in close contact with a particular DNA (see section 2.3 for the acronyms of the molecules in each system). Similarly, the 16 subfigures in Figure 5 correspond to the 16 PEIs in the 4D-16P system, and the four curves in each subfigure describe the binding state of a PEI with the four DNAs. In Figure 4, at the beginning of the simulation, PEI A1−A4 and DNA A constitute one D-4P complex, and PEI B1−B4 and DNA B constitute the other D-4P complex. Except for B1 and B2, each PEI has at least brief periods during which it forms a polyion bridge between the two DNAs (see section 2.3 for definition of "polyion bridge"). The bridges are transient; they form and break during the simulations. For example, the bridge formed by PEI A1 breaks for several times at around 25, 40, 70, and 85 ns. Notably, PEIs A1 and B4 contribute to the aggregation of the two DNAs significantly, each having more than 1 Ns in close contact with each DNA for longer than 50% of the entire simulation time. At around 60 ns, PEI A1 has as many as 4 Ns in close contact with each DNA. The same happens to PEI B4 at around 50 ns. Figure 5 demonstrates the polyion bridging in the 4D-16P system. Out of the 16 PEIs, 8 PEIs (A1, A3, B1, B4,
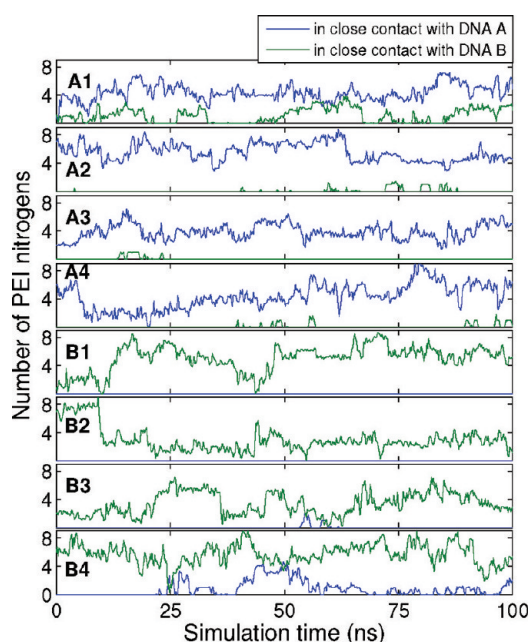
Figure 4. Number of nitrogens for each PEI within 4 Å of any N/O atom of each DNA as a function of time for the 2D-8P system which contains 2 DNAs and 8 PEIs. The 8 subfigures correspond to the 8 PEIs in the system; the 2 curves in each subfigure correspond to the 2 DNAs in the system.

C1, C3, C4, and D4) participate in bridging two or three DNAs for longer than 50% of the simulation time. In fact, the fraction of PEIs that contribute to bridging has increased from 25% in 2D-8P to 50% in 4D-16P. DNAs A, B, and C are mutually bridged (A and B bridged by PEIs A3, B4, C3; A and C bridged by PEIs A1, A2, C3, C4; B and C bridged by PEIs B3, C1, C3), while DNA D is only bridged with DNA B by PEIs B1 and D4. Noticeably, PEI C3 is bridging three DNAs (A, B, and C) from ∼30 ns until the end of the simulation.

The above results clearly demonstrate the presence of bridging PEIs when a DNA aggregate is formed. The bridging PEIs are not "locked" in bound state (see section 2.3 for definition of "bound") and undergo reversible binding. The polyion bridging
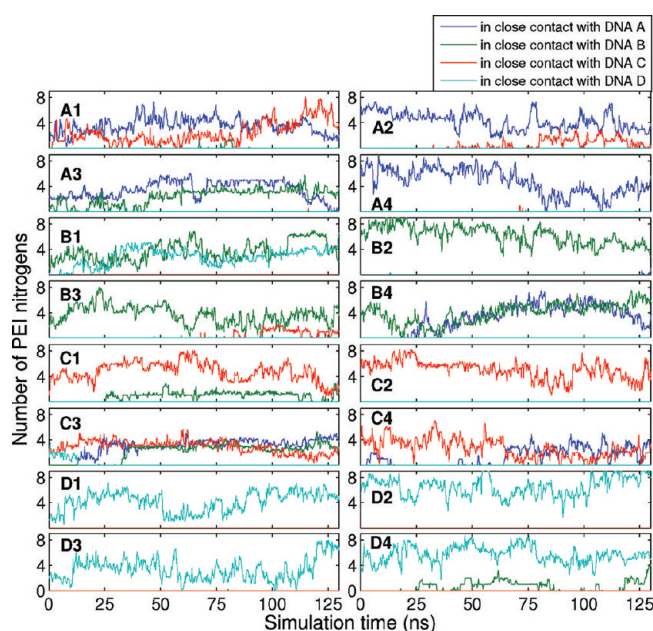
Figure 5. Number of nitrogens for each PEI within 4 Å of any N/O atom of each DNA as a function of time for the 4D-16P system which contains 4 DNAs and 16 PEIs. The 16 subfigures correspond to the 16 PEIs in the system; the 4 curves in each subfigure correspond to the 4 DNAs in the system.
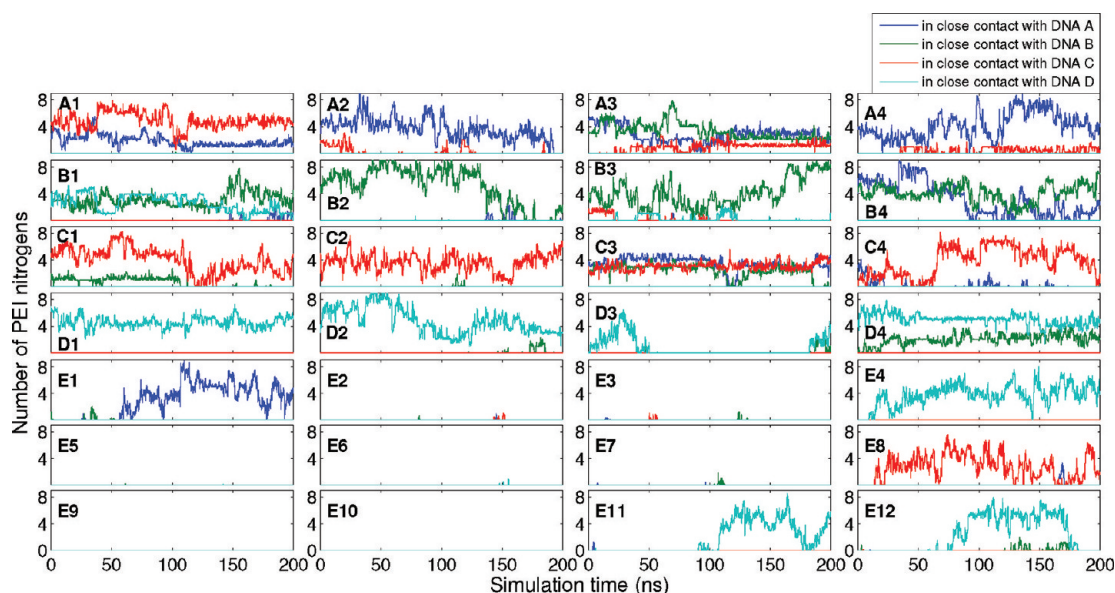

Figure 6. Number of nitrogens for each PEI within 4 Å of any N/O atom of each DNA as a function of time for the 2D-2P system which contains 2 DNAs and 2 PEIs. The 2 subfigures correspond to the 2 PEIs in the system; the 2 curves in each subfigure correspond to the 2 DNAs in the system.

is likely one of the key mechanisms causing the DNA aggregation. Another possible mechanism can be the electrostatic screening of DNA charges by PEIs at a short distance from the DNA surface so that the strong repulsive electrostatic interaction between DNAs at close separation is weakened (or shielded). To verify this, we performed the simulation of a system with a lower PEI to DNA charge ratio. The objective is to test if aggregation can remain with fewer PEIs, i.e., with less electrostatic screening. One way to do so is to start a new simulation as we did for 2D-8P, i.e., separate two DNA/PEI complexes first and check if they aggregate; however, one can encounter the same problem as we experienced in simulating 2D-8P-50. That is, the DNA aggregation could happen, while it might not be observed within the simulation time limited by current computational capability. As an alternative, we simulated the system 2D-2P with two DNAs and two PEIs following the procedure described in section 2.1; i.e., we made use of the final configuration from the 2D-8P simulation, kept the two PEIs bridging the two DNAs (PEIs A1 and B4), and replaced the other 6 PEIs with Na$^+$ ions. If the aggregate becomes looser or breaks, then the role of electrostatic screening will be verified. By visually checking the configurational change during the simulation, we observed loosening of the aggregate during the simulation (Figure 3c) and ultimate breakup of the aggregate at around 150 ns as seen in Figure 3d (also see movie "2D-2P.mpg" in Supporting Information). Figure 6 plots the number of Ns of each PEI in close contact with each DNA for 2D-2P. It can be seen that the polyion bridge lasts for 150 ns before it breaks and is not restored after the breakage. Clearly, the electrostatic screening of the PEI molecules also plays an important role in maintaining the DNAs in an aggregated form.

In experiments, the DNA/PEI complex is typically prepared in excess of PEIs. To examine DNA aggregation in excess of PEIs, we performed the simulation of 4D-28P by adding 12
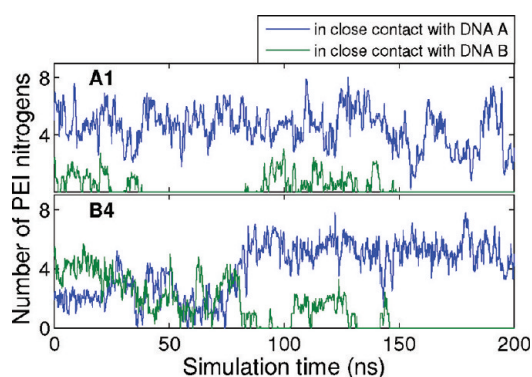
extra PEIs to the 4D-16P system at 100 ns and setting this time to be zero for the 4D-28P simulation. Figure 7 shows the number of Ns from each PEI in close contact with the DNAs in the 200 ns simulation. It can be seen that the polyion bridging between DNAs follows a similar characteristic as in 4D-16P. Eight out of the 28 PEIs (A1, A3, A4, B1, B4, C1, C3, and D4) participate in bridging two or three DNAs for longer than 50% of the simulation time. PEIs A3 and C3 are bridging three DNAs for most of the simulation time. Five out of the added 12 PEIs (E1, E4, E8, E11, and E12) bind with the DNAs for significantly long periods; however, they mainly bind with one DNA with only very short time windows to bridge two DNAs. For example, PEI E8 is only bound to DNA C over most time of the simulation while bridging DNAs A and C for several ns at ~170 ns. Noticeably, some of the original 16 PEIs were "replaced" by the added PEIs in that they unbound from the DNAs while allowing the newly added PEIs to form the DNA binding. For example, PEI D3 was replaced during the time window of 50−180 ns (also, see movie "4D-28P.mpg" in Supporting Information). Seven of the added PEIs (E2, E3, E5, E6, E7, E9, and E10) make no or negligible contact with the aggregate during the simulation. By studying the binding state of each PEI to each DNA in the 4D-28P system, we found that ~18 PEIs were bound with the DNAs at the late stage of the simulation (see Figure S1 in Supporting Information). As the 18 PEIs carry a total charge of +108 and the 4 DNAs carry a total charge of −88, the formed DNA/PEI aggregate is even more positively charged than the aggregate obtained in the 4D-16P system which carries a net charge of +8. This is consistent with the experimental measurements of the ζ-potential of DNA/PEI complexes; it is well established that the gradual addition of PEI molecules results in a progressive increase in ζ-potential, ultimately reaching >+30 mV in the presence of excess PEI and indicating cationic nature of the final aggregates.[7]

3.2. Charge Neutralization. As demonstrated in section 3.1, electrostatic screening plays an crucial role in DNA aggregation. To investigate how PEIs neutralize the DNA charges, we plotted the cumulative distributions, with respect to the DNA C1′ atoms, of protonated PEI Ns, Na$^+$/Cl$^-$ ions, and the net charge of PEI and ions, averaged over the last 40 ns of the simulations (Figure 7). The C1′ atoms are on the sugar rings of the DNAs, located inside the DNA helix at a distance of ~5 Å from the surface of DNA defined by the phosphorus

Figure 7. Number of nitrogens for each PEI within 4 Å of any N/O atom of each DNA as a function of time for the 4D-28P system which contains 4 DNAs and 28 PEIs. The 28 subfigures correspond to the 28 PEIs in the system; the 4 curves in each subfigure correspond to the 4 DNAs in the system.

atoms (see Figure S2 in Supporting Information). In systems D-4P, 2D-8P, and 4D-16P, the DNA/PEI charge ratio is approximately 1/1; in systems D-8P and 4D-28P, the DNA/PEI charge ratio is approximately 1/2; and in system 2D-2P, the DNA/PEI charge ratio is approximately 4/1. In each subfigure of Figure 8, the straight dashed black line indicates
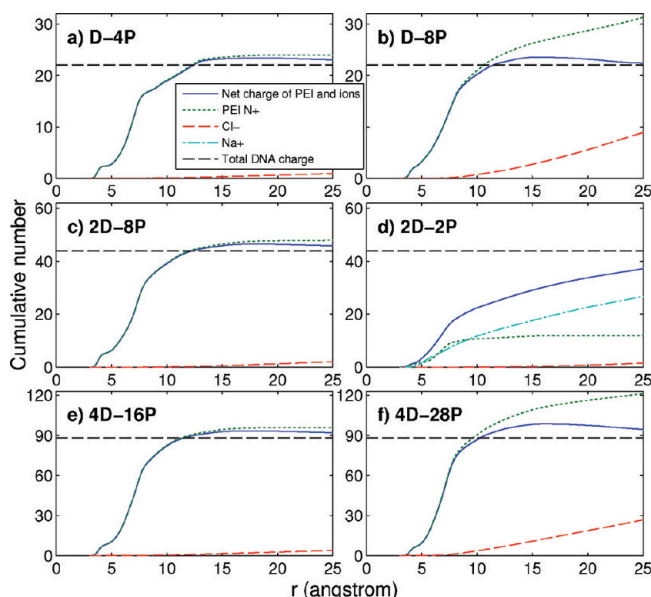

Figure 8. Cumulative numbers of protonated PEI nitrogens, Na^+, Cl^-, and net charge of PEI/Na^+/Cl^- as a function of the distance from any C1′ DNA atom (averaged over the last 40 ns of each simulation). The total charge of all the DNAs in each system is plotted by a straight dashed black lines as reference. (a) D-4P, (b) D-8P, (c) 2D-8P, (d) 2D-2P, (e) 4D-16P, (f) 4D-28P.

the total charge all the DNAs in the system carry, and the blue solid curve is the total charge of PEI and ions within given distance to their nearest DNA C1′ atoms. If the black line and blue curve intersect, the DNA charges are 100% neutralized by

the PEI and ions at the distance where they intersect. At larger distances, the PEI and ions charges could exceed the DNA charges, and the DNA would be "overneutralized" at such distances. This is the case for the five systems in Figure 8, except the 2D-2P system. It can be seen, for these five systems, with DNA/PEI charge ratio of 1/1 or 1/2, the curves for the net charge of PEI and ions have a similar characteristic. That is, the DNA(s) are 50% neutralized at a distance of ~7 Å and 100% neutralized at a distance of ~12 Å from their C1′ atoms; the DNA(s) are slightly "overneutralized" beyond the distance of ~12 Å from their C1′ atoms and the "overneutralization" maximize at ~15 Å. For systems D-4P, 2D-8P, and 4D-16P, all the PEI charges are located within 15 Å from the DNA C1′ atoms, supported by the observation that the cumulative number of PEI N^+ is constant beyond 15 Å. For systems D-8P and 4D-28P, more PEI charges still accumulate gradually beyond 15 Å, which however are largely neutralized by Cl^-. The scenario for 2D-2P is very different from the other five cases. The DNAs are not fully neutralized even at a distance of 25 Å from their C1′ atoms; all the 12 charges from the two PEIs are within 8 Å from the DNA C1′ atoms, and the DNAs are only about 50% neutralized at a distance of 12 Å from their C1′ atoms. This demonstrates that PEI is much more capable of neutralizing the DNA at a short distance from the DNA surface than monovalent ions. We have also plotted the cumulative net charge of PEI/Na^+/Cl^- based on three time windows at the late stage of the simulations as an evidence of convergence of the simulation trajectories (see Figure S4 in Supporting Information).

3.3. DNA–DNA Spacing in the Aggregate. The DNA–DNA spacing reflects the compactness of DNA molecules in the aggregate and has been a great interest of experimental studies.[1,17,41,42] The DNA–DNA spacing from our MD trajectories was analyzed, and Figures 9–12 show the distance between any two DNA molecules as a function of simulation time for the 2D-8P, 2D-2P, 4D-16P, and 4D-28P systems, respectively (see section 2.3 for the definitions of "shortest distance" and "rms distance").
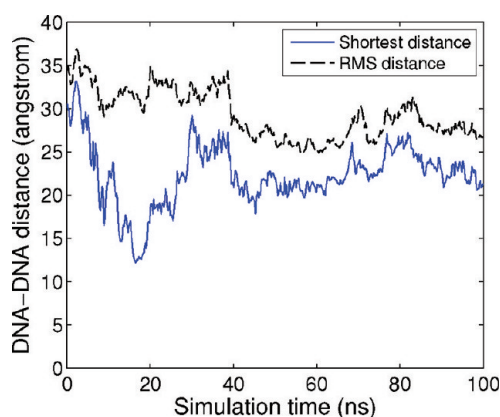
Figure 9. DNA−DNA distance in the 2D-8P system which contains two DNAs: (a) shortest distance; (b) root mean square distance (see texts for definition of these distances).

In Figure 9 for the 2D-8P system, it can be seen the two curves decrease at the beginning of the simulation, indicating the approach of the two DNAs. The curves flatten after 40 ns with the average values of ∼23 Å for the $d_{shortest}$ and ∼28 Å for the d_{rms}. In Figure 10 for the 2D-2P system, the two curves
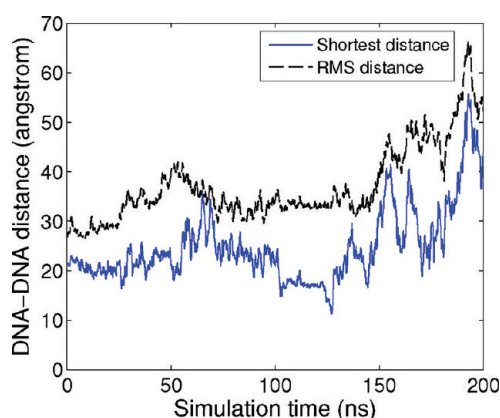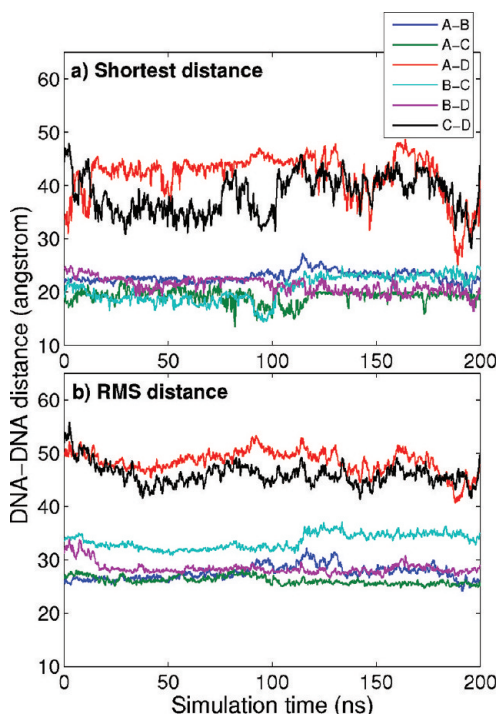

Figure 10. DNA−DNA distance in the 2D-2P system which contains two DNAs: (a) shortest distance; (b) root mean square distance (see texts for definition of these distances).

remain relatively stable without significant fluctuation from 0 to 150 ns when the two DNAs are still bridged by one or two PEIs. At about 150 ns when the polyion bridge breaks, the two curve increase dramatically, indicating the separation of the two DNAs. In Figure 11 for 4D-16P, we observe a similar characteristic as seen in Figure 9 for the pairs of DNAs bridged by PEIs (A−B, A−C, B−C, B−D), while, for the pairs of DNAs not bridged by PEIs (A−D, C−D), the d_{rms} and $d_{shortest}$ values are much larger than 23 and 28 Å. In Figure 12 for the 4D-28P system, the curves for the DNA pairs bridged by PEIs (A−B, A−C, B−C, B−D) remain almost constants during the entire 200 ns simulation, with fluctuations at a similar magnitude as their counterparts in the 4D-16P system after 50 ns. The DNAs pairs not bridged in the 4D-16P system (A−D, C−D) stayed separate during the simulation of the 4D-28P system. This demonstrates that the added PEIs, although can bind to the DNAs and even replace the previously attached PEIs as shown earlier, do not affect the DNA−DNA spacing in the aggregate.

During the simulations, $d_{shortest}$ of two DNAs can be less than 20 Å, such as the DNA pair in the 2D-8P system at around
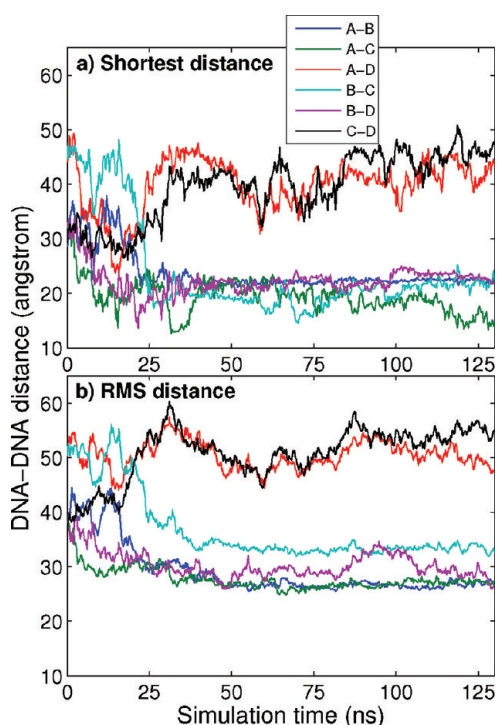
Figure 11. DNA−DNA distances in the 4D-16P system which contains four DNAs (A, B, C, and D): (a) shortest distance; (b) root mean square distance (see texts for definition of these distances).

Figure 12. DNA−DNA distances in the 4D-28P system which contains four DNAs (A, B, C, and D): (a) shortest distance; (b) root mean square distance (see texts for definition of these distances).

18 ns ($d_{shortest}$ ∼ 12 Å) and the DNA pair A-C in the 4D-16P system at around 30 and 120 ns ($d_{shortest}$ ∼ 15 Å). This is unexpected as the diameter of a DNA molecule is about 20 Å. By further examining the simulation trajectories, it was revealed that the two DNAs adopted an L or T shape arrangement with

Table 3. DNA−DNA Distance Averaged over the Last 40 ns of the Simulations (Å)

DNA−DNA	2D-8P	4D-16P				4D-28P				
	A−B	A−B	A−C	B−C	B−D	A−B	A−C	B−C	B−D	av
$d_{shortest}$	23.2	22.3	17.1	21.4	23.1	22.7	19.4	23.1	20.0	21.4
d_{rms}	27.7	26.7	27.1	33.3	29.9	27.3	25.5	34.7	28.4	29.0

one end of a DNA nearly perpendicular to the other DNA (see Figure S3 in Supporting Information). In such configurations, $d_{shortest}$ does not reflect the shortest interduplex distance of DNA segments in compact plasmid DNAs, which is the distance between the axes of two parallel DNA segments. Table 3 summarizes average $d_{shortest}$ and d_{rms} during the last 40 ns of the simulations for the bridged DNA pairs in the 2D-8P, 4D-16P and 4D-28P systems. Average $d_{shortest}$ for the 9 pairs of DNAs is 21.4 Å, and average d_{rms} is 29.0 Å. Because of the special configurations mentioned above for the short DNAs simulated in this work, the actual average DNA−DNA spacing in plasmid DNA/PEI complex should be larger than the average $d_{shortest}$ (21.4 Å). As d_{rms} in our calculations characterizes the average distance between two short DNAs that may not have parallel axes, the average DNA−DNA spacing in plasmid DNA/PEI complex should be smaller than the average d_{rms} (29.0 Å) obtained here. Hence, we believe that the average DNA−DNA spacing in plasmid DNA/PEI complex should be between 21.4 and 29.0 Å. The DNA interduplex distance in bacteriophages is ~27 Å,[41] and that for DNAs wrapped around the histone core of nucleosomes was also found to be ~27 Å.[1] Our simulation results demonstrate that the DNAs in the DNA/PEI complex are as compact as those in bacteriophages and nucleosomes. The spacing between DNAs condensed by 35 kDa poly(L-arginine) was reported to be ~28 Å in a recent experimental study,[17] within the range of spacing obtained from our simulations. We have also plotted the radii of gyration of the DNAs in each aggregates (see Figure S5 in Supporting Information), which generally follow a similar trend as "rms distance" shown in Figures 9−12.

3.4. Implications. On the theoretical front of investigating DNA aggregation, Savelyev and Papoian studied the inter-DNA interaction in NaCl and KCl solution using all-atom MD simulations and generated the repulsive interaction potential profiles of two parallel DNA oligomers.[43] Dai et al. performed a series of all-atom MD simulations to study DNA attraction mediated by multivalent ions including putrescine (2+), spermidine (3+), spermine (4+), and cobalt hexamine (3+), the inter-DNA interaction potential profiles were calculated, and the dynamics of the complexes was investigated.[44] The above two works, however, only studied the inter-DNA interaction mediated by monovalent and multivalent ions. To the best of our knowledge, the work presented here is the first all-atom MD simulation of cationic polymer mediated DNA aggregation involving multiple DNA molecules.

Our simulations revealed dynamics of the PEI mediated DNA aggregation, which is unaccessible through experiments. It is likely that the obtained results will be applicable to other polymeric carriers apart from PEI. During the simulations of DNA-PEI aggregation, bridging PEIs were observed connecting multiple DNA molecules even though they were initially confined to a single DNA molecule. The number and binding strength of such bridging PEIs are likely to dictate the stability of aggregates. The bridging PEIs, however, were found to be highly dynamic and the binding to multiple DNA molecules were reversible. Only a select number of PEIs participated in

DNA bridging and some remained exclusively committed to DNA molecules that they were originally bound to (within the limitation of simulation times). A critical PEI/DNA ratio was needed for stable aggregation; whereas 4 PEI molecules/DNA (corresponding to mass ratio of ~0.31) gave stable complexes, 1 PEI molecule/DNA (corresponding to mass ratio of ~0.08) was found insufficient to maintain DNA aggregation. Under experimental conditions, we previously reported a polymer/DNA mass ratios of ~0.4 for complete DNA binding irrespective of the molecular weight of PEI.[45] Since almost complete DNA binding by carriers is a prerequisite for DNA aggregation, the simulations results were consistent with the experimentally investigated DNA aggregation. It was worthwhile to note that aggregation successfully occurred even though there was a net positive charge for individual PEI/DNA complexes (each D-4P complex carries a net charge of +2). Local attractive forces have compensated for the overall repulsive force associated with like-charged entities. An overall positive charge is typically observed in PEI/DNA complexes prepared with excess PEI,[7] and in this regard, our simulations concurred with the experimental observations.

A significant observation derived from the current studies was the ability of free PEI molecules to replace PEI molecules already bound to DNA molecules in an aggregate. This process will have implications for preparation of DNA complexes to be used for transfection, as well as for dissociation of DNA complexes essential for functional transfection. The fact that excess DNA-binding molecules might displace already bound molecules might be utilized to better engineer DNA complexes prepared by step-by-step addition of transfection complexes,[46] where complexes are prepared by sequential addition of constituent molecules. For example, A−B−C−D complexes were prepared by complexing DNA (A) with polymeric polycations (B), followed by the addition of lipophilic substituents (C) and cell-binding moieties (D). Our results support the experimental observation that such sequential addition of DNA-binding molecules can lead to stable incorporation of individual constituents added at later stages of assembly. Optimizing the complex properties in this approach were mostly experimentally driven, and the current study provide an alternative means to further fine-tune the bound state of the complexes. It might be possible to compare the relative binding affinity of substituents *in silico* beforehand and determining which molecules might be more stably incorporated into the complexes. The final state of the specific molecules in the complexes might be better understood in this way. For example, MD simulations could be used to determine if cell-binding moieties are embedded in a complex or retained on the surface readily accessible for target binding.

Macromolecular displacement of DNA-binding molecules in aggregates might be especially critical for complex stability. Interaction with naturally occurring macromolecules in the extracellular matrix (e.g., heparan sulfate) has undesirable consequence on transfection,[47,48] which leads to inhibition of DNA uptake. MD simulations can help identify DNA carriers resistant to such displacements and enhance the stability of

DNA aggregates that is needed for cellular uptake. Displacement with intracellular macromolecules, on the other hand, is essential to release the DNA in free form for efficient transcription.[49,50] Specific proteins capable of interacting with DNA complexes were identified,[51,52] whose binding to complexes were shown to facilitate nuclear uptake and ultimately transgene expression. The atomistic MD simulations might shed important insight into this process, providing a better means to predict the complex stability in the presence of these intracellular molecules. Simulating displacement of carrier molecules with known DNA-binding molecules such as histones will reveal information about DNA disassembly inside the cells.

3.5. Limitations and Future Studies. Even though the simulations reported here are the-state-of-the-art in terms of model size and simulation time, the current computational limitations restricted us to focusing on only one species of PEI, where the protonation state, architecture, and molecular weight were fixed. Such factors can potentially affect PEI mediated DNA aggregation and will be part of our future work. We already know that PEIs with lower degree of protonation display lower binding affinity to DNA (i.e., binding is less stable in MD simulations).[31] The linear form of the PEI also behaves in a similar fashion as compared to the branched PEIs simulated here.[31] The level of protonation employed in this study was more realistic of PEI's state under physiological conditions (i.e., pH between 6 and 7),[30] and branched PEI is more commonly used for DNA delivery. On the basis of our past simulations for 23% protonated PEIs,[31] which mimics PEI's state at pH 8,[30] several conjectures can be made on DNA aggregation by the less protonated PEIs. First, due to their lower binding affinity to DNA,[31] the aggregates mediated by less protonated PEIs would be less stable and the PEI exchange among the DNA molecules might be more common. Because a considerable fraction of Ns in 23% PEIs contribute to binding with DNA through indirect hydrogen bonding mediated by water molecules,[31] we expect the 23% PEIs to neutralize the DNA at a larger distance from the DNA C1′ atoms compared with the 46% PEIs; i.e., the capability of 23% PEIs to neutralize the DNA would be weaker. This might cause the formed aggregate in excess PEIs to be less positively charged. The looser binding of 23% PEI to DNA may also increase the DNA−DNA spacing in the aggregate. These conjectures will be tested via additional simulations.

Another limitation is the size of DNA aggregates studies here, where the largest aggregate was composed of 4 DNA molecules leading to a size of ∼10 nm with excess PEIs. The aggregate size formed with the PEI/DNA complexes are larger in reality. For example, ∼100 nm aggregates are routinely reported for the 25 kDa branched PEI, and we recently reported aggregates as large as 500−700 nm for the PEIs with MW of 0.6−2.0 kDa.[45] Therefore, a larger numbers of DNA complexes will be needed to realistically simulate DNA aggregation employed for cell transfections. Alternatively, longer chain DNA molecules might be needed to achieve more realistic aggregation. MD simulations can help understand what determines the aggregate size obtained under experimental conditions and, more importantly, what makes the aggregation stop before an exuberant aggregate is formed consuming all of the DNA and PEI molecules. Since size is important in the transfection efficiency of the DNA aggregates,[53,54] better control of transfection could be achieved as a result of such simulations.

4. CONCLUSIONS

We performed a series of all-atom MD simulations to study PEI mediated DNA aggregation. The results clearly demonstrate that PEIs contribute to DNA aggregation through two mechanisms: (i) forming polyion bridges between DNA segments and (ii) screening the negative DNA charges at a short distance from the surface of DNA molecules. As a consequence of the latter mechanism, the PEI/DNA charge ratio needs to be above certain value in order to maintain a stable aggregation. Compared with monovalent ions, PEIs are shown to be more capable of neutralizing the DNAs at close distance and provide full neutralization at ∼12 Å from the DNA C1′ atoms, when the PEI/DNA charge ratio is above 1. The DNA−DNA spacing in the DNA/PEI aggregates were between 21.4 and 29.0 Å. Excess PEIs were capable of binding to the already positively charged aggregate and further increase its charge. They can also replace the PEIs previously bound to the DNAs in the aggregate. The binding of excess PEIs, however, does not change the DNA−DNA spacing.

■ ASSOCIATED CONTENT

Ⓢ Supporting Information
Movies of simulation trajectories; additional figures. This material is available free of charge via the Internet at http://pubs.acs.org.

■ AUTHOR INFORMATION

Corresponding Author
*E-mail: tian.tang@ualberta.ca. Phone: +1-780-492-5467. Fax: +1-780-492-2200.

■ ACKNOWLEDGMENTS

■ REFERENCES

(1) Luger, K.; Mader, A.; Richmond, R.; Sargent, D.; Richmond, T. *Nature* **1997**, *389*, 251−260.

(2) Luo, D.; Saltzman, W. *Nature Biotechnol.* **2000**, *18*, 33−37.

(3) Boussif, O.; Lezoualc'h, F.; Zanta, M. A.; Mergny, M. D.; Scherman, D.; Demeneix, B.; Behr, J. P. *Proc. Natl. Acad. Sci. U. S. A.* **1995**, *92*, 7297−7301.

(4) Godbey, W.; Wu, K.; Mikos, A. *J. Controlled Release* **1999**, *60*, 149−160.

(5) Kwok, A.; Hart, S. L. *Nanomedicine* **2011**, *7*, 210−219.

(6) Abbasi, M.; Uludag, H.; Incani, V.; Hsu, C. Y. M.; Jeffery, A. *Biomacromolecules* **2008**, *9*, 1618−1630.

(7) Bahadur, K. C. R.; Landry, B.; Aliabadi, H. M.; Lavasanifar, A.; Uludag, H. *Acta Biomater.* **2011**, *7*, 2209−2217.

(8) Bertschinger, M.; Schertenleib, A.; Cevey, J.; Hacker, D. L.; Wurm, F. M. *Mol. Biotechnol.* **2008**, *40*, 136−143.

(9) Bertschinger, M.; Backliwal, G.; Schertenleib, A.; Jordan, M.; Hacker, D. L.; Wurm, F. M. *J. Controlled Release* **2006**, *116*, 96−104.

(10) Stevens, M. *Biophys. J.* **2001**, *80*, 130−139.

(11) Winkler, R.; Steinhauser, M.; Reineker, P. *Phys. Rev. E* **2002**, *66*, 021802.

(12) Hayashi, Y.; Ullner, M.; Linse, P. *J. Chem. Phys.* **2002**, *116*, 6836−6845.

(13) Hayashi, Y.; Ullner, M.; Linse, P. *J. Phys. Chem. B* **2003**, *107*, 8198−8207.

(14) Hayashi, Y.; Ullner, M.; Linse, P. *J. Phys. Chem. B* **2004**, *108*, 15266−15277.

(15) Dias, R.; Pais, A.; Miguel, M.; Lindman, B. *J. Chem. Phys.* **2003**, *119*, 8150−8157.

(16) Ziebarth, J.; Wang, Y. *J. Phys. Chem. B* **2010**, *114*, 6225−6232.

(17) DeRouchey, J.; Parsegian, V. A.; Rau, D. C. *Biophys. J.* **2010**, *99*, 2608−2615.

(18) Li, L.; Pabit, S. A.; Meisburger, S. P.; Pollack, L. *Phys. Rev. Lett.* **2011**, *106*.

(19) Qiu, X.; Parsegian, V. A.; Rau, D. C. *Proc. Natl. Acad. Sci. U. S. A.* **2010**, *107*, 21482−21486.

(20) Ziebarth, J.; Wang, Y. *Biophys. J.* **2009**, *97*, 1971−1983.

(21) Pavan, G. M.; Danani, A.; Pricl, S.; Smith, D. K. *J. Am. Chem. Soc.* **2009**, *131*, 9686−9694.

(22) Pavan, G. M.; Kostiainen, M. A.; Danani, A. *J. Phys. Chem. B* **2010**, *114*, 5686−5693.

(23) Pavan, G. M.; Albertazzi, L.; Danani, A. *J. Phys. Chem. B* **2010**, *114*, 2667−2675.

(24) Pavan, G. M.; Mintzer, M. A.; Simanek, E. E.; Merkel, O. M.; Kissel, T.; Danani, A. *Biomacromolecules* **2010**, *11*, 721−730.

(25) Ouyang, D.; Zhang, H.; Herten, D.-P.; Parekh, H. S.; Smith, S. C. *J. Phys. Chem. B* **2010**, *114*, 9220−9230.

(26) Ouyang, D.; Zhang, H.; Parekh, H. S.; Smith, S. C. *J. Phys. Chem. B* **2010**, *114*, 9231−9237.

(27) Ouyang, D.; Zhang, H.; Parekh, H. S.; Smith, S. C. *Biophys. Chem.* **2011**, *158*, 126−133.

(28) Jere, D.; Jiang, H. L.; Arote, R.; Kim, Y. K.; Choi, Y. J.; Cho, M. H.; Akaike, T.; Chot, C. S. *Expert Opin. Drug Delivery* **2009**, *6*, 827−834.

(29) Aliabadi, H. M.; Landry, B.; Bahadur, R. K.; Neamnark, A.; Suwantong, O.; Uludag, H. *Macromol. Biosci.* **2011**, *11*, 662−672.

(30) Utsuno, K.; Uludag, H. *Biophys. J.* **2010**, *99*, 201−207.

(31) Sun, C.; Tang, T.; Uludag, H.; Cuervo, J. E. *Biophys. J.* **2011**, *100*, 2754−2763.

(32) Sun, C.; Tang, T. *J. Adhes. Sci. Technol.* **2011**, in press.

(33) Vanommeslaeghe, K.; Hatcher, E.; Acharya, C.; Kundu, S.; Zhong, S.; Shim, J.; Darian, E.; Guvench, O.; Lopes, P.; Vorobyov, I.; MacKerell, A. D. Jr. *J. Comput. Chem.* **2010**, *31*, 671−690.

(34) Brooks, B.; Bruccoleri, R.; Olafson, D.; States, D.; Swaminathan, S.; Karplus, M. *J. Comput. Chem.* **1983**, *4*, 187−217.

(35) MacKerel Jr., A.; Brooks III, C.; Nilsson, L.; Roux, B.; Won, Y.; Karplus, M. In *CHARMM: The Energy Function and Its Parameterization with an Overview of the Program*; v. R. Schleyer, P., et al., Eds.; The Encyclopedia of Computational Chemistry; John Wiley & Sons: Chichester, 1998; Vol. *1*, pp 271−277.

(36) Phillips, J.; Braun, R.; Wang, W.; Gumbart, J.; Tajkhorshid, E.; Villa, E.; Chipot, C.; Skeel, R.; Kale, L.; Schulten, K. *J. Comput. Chem.* **2005**, *26*, 1781−1802.

(37) Jorgensen, W. *J. Am. Chem. Soc.* **1981**, *103*, 335−340.

(38) Darden, T.; York, D.; Pedersen, L. *J. Chem. Phys.* **1993**, *98*, 10089−10092.

(39) Ryckaert, J.; Ciccotti, G.; Berendsen, H. *J. Comput. Phys.* **1977**, *23*, 327−341.

(40) Humphrey, W.; Dalke, A.; Schulten, K. *J. Mol. Graphics* **1996**, *14*, 33−38.

(41) Cerritelli, M.; Cheng, N.; Rosenberg, A.; McPherson, C.; Booy, F.; Steven, A. *Cell* **1997**, *91*, 271−280.

(42) Qiu, X.; Rau, D. C.; Parsegian, V. A.; Fang, L. T.; Knobler, C. M.; Gelbart, W. M. *Phys. Rev. Lett.* **2011**, *106*, 028102.

(43) Savelyev, A.; Papoian, G. A. *J. Am. Chem. Soc.* **2007**, *129*, 6060−6061.

(44) Dai, L.; Mu, Y.; Nordenskiöld, L.; van der Maarel, J. R. C. *Phys. Rev. Lett.* **2008**, *100*, 118301.

(45) Bahadur, R.K. C.; Uludag, H. *J. Biomater. Sci., Polym. Ed.* **2011**, *22*, 873−892.

(46) Kostarelos, K.; Miller, A. *Chem. Soc. Rev.* **2005**, *34*, 970−994.

(47) Shim, M. S.; Wang, X.; Ragan, R.; Kwon, Y. *J. Microsc. Res. Tech.* **2010**, *73*, 845−856.

(48) Danielsen, S.; Strand, S.; Davies, C.; Stokke, B. *Biochim. Biophys. Acta* **2005**, *1721*, 44−54.

(49) Thibault, M.; Nimesh, S.; Lavertu, M.; Buschmann, M. D. *Mol. Ther.* **2010**, *18*, 1787−1795.

(50) Chen, H. H.; Ho, Y.-P.; Jiang, X.; Mao, H.-Q.; Wang, T.-H.; Leong, K. W. *Mol. Ther.* **2008**, *16*, 324−332.

(51) Munkonge, F. M.; et al. *J. Biol. Chem.* **2009**, *284*, 26978−26987.

(52) Kaouass, M.; Beaulieu, R.; Balicki, D. *J. Controlled Release* **2006**, *113*, 245−254.

(53) Kunath, K.; von Harpe, A.; Fischer, D.; Kissel, T. *J. Controlled Release* **2003**, *88*, 159−172.

(54) Higuchi, Y.; Kawakami, S.; Fumoto, S.; Yamashita, F.; Hashida, M. *Biol. Pharm. Bull.* **2006**, *29*, 1521−1523.